


## Article

# Enhancing Vapochromic Properties of Platinum(II) Terpyridine Chloride Hexafluoro Phosphate in Terms of Sensitivity through Nanocrystalization for Fluorometric Detection of Acetonitrile Vapors

Sedigheh Barzegar <sup>1,2</sup>, Mahmood Karimi Abdolmaleki <sup>3,\*</sup> , William B. Connick <sup>2</sup> and Ghodratollah Absalan <sup>1</sup><sup>1</sup> Massoumi Laboratory, Department of Chemistry, College of Sciences, Shiraz University, Shiraz 71454, Iran; sedighechem62@yahoo.com (S.B.)<sup>2</sup> Department of Chemistry, University of Cincinnati, Cincinnati, OH 45221, USA<sup>3</sup> Department of Physical and Environmental Sciences, Texas A&M University-Corpus Christi, 6300 Ocean Drive, Corpus Christi, TX 78412, USA

\* Correspondence: ben.karimi@tamucc.edu

**Abstract:** The vapochromic properties of [Pt(tpy)Cl](PF<sub>6</sub>) crystals in the presence of acetonitrile and its effect on the crystal structure as well as the fluorescence spectrum of this complex have already been studied in the past. We synthesized nanocrystals of this compound for the first time, and discussed different parameters and methods that affect nanocrystal structure modulation. The study demonstrates the vapochromic properties of the nanocrystals toward acetonitrile vapor by investigating the morphology and fluorescence spectra of the nanocrystals. Vapochromic studies were conducted on [Pt(tpy)Cl](PF<sub>6</sub>) nanocrystals for five cycles of absorption and desorption of acetonitrile, demonstrating shorter response times compared to regular bulk crystals.

**Keywords:** Pt(II) complex; [Pt(tpy)Cl](PF<sub>6</sub>) crystals; [Pt(tpy)Cl](PF<sub>6</sub>) nanocrystals; vapochromic crystals; vapochromic nanocrystals



**Citation:** Barzegar, S.; Karimi Abdolmaleki, M.; Connick, W.B.; Absalan, G. Enhancing Vapochromic Properties of Platinum(II) Terpyridine Chloride Hexafluoro Phosphate in Terms of Sensitivity through Nanocrystalization for Fluorometric Detection of Acetonitrile Vapors. *Crystals* **2024**, *14*, 347. <https://doi.org/10.3390/cryst14040347>

Academic Editors: Andrew F. Zhou and Peter X. Feng

Received: 22 February 2024

Revised: 25 March 2024

Accepted: 29 March 2024

Published: 5 April 2024



**Copyright:** © 2024 by the authors. Licensee MDPI, Basel, Switzerland. This article is an open access article distributed under the terms and conditions of the Creative Commons Attribution (CC BY) license (<https://creativecommons.org/licenses/by/4.0/>).

## 1. Introduction

Vapochromic and vapoluminescent materials have garnered significant scientific interest due to their potential applications as chemical sensors and modules for detecting various environmental factors such as temperature, pressure, and the concentration of chemical vapors, including volatile organic compounds (VOCs) [1–9]. Investigations in this area have reported the color, fluorescence, and/or phosphorescence change in vapochromic materials through adsorption and/or desorption of vapors [10–18]. For example, a study examined how [Pt(tpy)Cl](PF<sub>6</sub>) crystals change with the exposure to acetonitrile (MeCN), a VOC, and how this affects their structure [10]. Another study explored how exposure to water vapor causes a transition between hydrated and dehydrated forms of Pt(tpy)ClClO<sub>4</sub>, a square-planar Pt(II) complex, with reversible spectroscopic changes, indicating recyclability [19]. Additionally, research on three specific square-planar Pt(II) complexes found that exposure to VOC vapors induces luminescent switching properties in all three complexes [20].

This vapochromic/vapoluminescent phenomenon occurs due to the splitting of the complex ligand field and the alteration of distances between the Pt(II) ions in square-planar Pt(II) complexes. However, designing a vapor-sensitive and selective sensor with these properties has remained challenging [10,21]. The spectroscopic characteristics of square planar Pt(II) complexes stem from interactions between Pt atoms. These interactions, which are noncovalent, form quasi-one-dimensional stacked systems depending on the ligands incorporated into the complex [22,23]. Initially, the Pt(II) units in the parent solid complex have normal distances, but they rearrange into a continuous chain with short

Pt...Pt overlaps in the new lattice formed after exposure to vapor [10]. Any variation in these Pt...Pt interactions, caused by substitutions in the ligand and/or counterions as well as various intermolecular interactions (e.g., hydrogen bonds, coordination bonds, hydrophobic interactions), result in modulation of spectroscopic properties [24–27] due to the changes in the complex's lattice parameters. These changes in spectroscopic properties make these complexes suitable for use as sensors in analyte detection.

When VOCs fill the gaps in the lattice of the Pt(II) complex, they rearrange the Pt...Pt interaction, creating a new lattice. This rearrangement causes a change in the spectroscopic properties of the complex. VOCs can be detected sensitively and selectively because they match the size and shape of the voids [10]. Notably, VOCs are chemicals with high vapor pressures at room temperature, posing environmental risks and health hazards. Therefore, detecting them is crucially important.

Using fluorometry improves the vapochromic properties of the complex because fluorescence spectroscopy is approximately a thousand times more sensitive and selective compared to the UV/Vis absorption spectrophotometry. This increased sensitivity leads to better detection limits. Therefore, the main purpose of our study is to achieve more precise and accurate measurements. We synthesized nanocrystals of [Pt(tpy)Cl](PF<sub>6</sub>), to the best of our knowledge for the first time. We discuss various methods and parameters that influence the modulation of the nanocrystal structure. Then, we investigate the vapochromic properties of these nanocrystals in response to MeCN vapor by analyzing their morphology and fluorescence spectra after exposure to MeCN. This allows us to examine the differences in vapochromism between crystals and nanocrystals and determine their suitability for use in vapor sensors.

## 2. Experimental

### 2.1. Reagents

We purchased K<sub>2</sub>PtCl<sub>4</sub> from Pressure Chemical, while both COD (1,5-cyclooctadiene) and tpy (2,2':6'2''-terpyridine) were obtained from Aldrich. Additionally, NH<sub>4</sub>PF<sub>6</sub> was purchased from Alfa Aesar, and acetonitrile (MeCN), acetone, acetic acid, and hexane were bought from Merck chemical company. Poly-alanine and sodium iodide were bought from Sigma and Fisher Scientific, respectively. Deionized water was utilized in all experiments.

### 2.2. Apparatus

We used an Acton SpectraPro 300i spectrophotometer equipped with a photon counter photomultiplier tube (PMT) detector to record the fluorescence spectra. Mass spectra were obtained using a Micromass Q-time of flight (TOF) 2 instrument from Waters, Milford, MA, USA. A Bruker AC 400 MHz NMR was used to characterize the synthesized compounds. SEM images of both crystals and nanocrystals were collected using an FEI/Phillip XL 30 ESEM-FEG from F.E.I. Company (Hillsboro, OR, USA). X-ray powder diffraction (XRD) patterns were acquired using a Philips X'Pert Powder Diffractometer from Malvern Panalytical company (Malvern, UK), employing 0.413620 Å photons in transmission setup. We used platinum striped mirrors to select incident photons, along with a double Si(111) monochromator featuring an adjustable sagittal focus. Scattered beams were filtered using (12) perfect Si(111) analyzer crystals. Discrete detectors spanning an angular range from −6 to 16° 2θ were scanned across a 34° 2θ range. Data points were collected at intervals of 0.001° 2θ, with a scanning speed set at 0.01°/s.

### 2.3. Synthesis of [Pt(tpy)Cl](PF<sub>6</sub>)

A total of 2.5 g of K<sub>2</sub>PtCl<sub>4</sub> was weighed and added to a round bottom flask. Then, 60.0 mL of water and 80.0 mL of acetic acid were added, and the mixture was left under an Ar bubble for 30 min. Afterward, 2.44 mL of COD was added using a syringe, and the mixture was refluxed for one hour. To obtain a precipitate, the solution was filtered under vacuum, and the obtained precipitate was washed with deionized water several times. The precipitate was then placed under low vacuum in the hood overnight to obtain a powder

of  $\text{Pt}(\text{COD})\text{Cl}_2$ . In the next step, 1.5 g of  $\text{Pt}(\text{COD})\text{Cl}_2$  and 0.94 g of 2,2':6'2''-terpyridine (tpy) were added to a 1000 mL round-bottom volumetric flask, followed by the addition of 800 mL water and 50 mL acetone. The mixture was refluxed with gentle stirring overnight to dissolve  $[\text{Pt}(\text{tpy})\text{Cl}]\text{Cl}$ . The solution was then transferred to a beaker, and a small amount of  $\text{NH}_4\text{PF}_6$  was added while the solution was still warm from the refluxing step. An emulsion of  $[\text{Pt}(\text{tpy})\text{Cl}](\text{PF}_6)$  was formed (Figure 1) as a yellow precipitate via an anion metathesis reaction between  $[\text{Pt}(\text{tpy})\text{Cl}]\text{Cl}$  and  $\text{NH}_4\text{PF}_6$  in water. The emulsion was filtered under vacuum to obtain a powdered form of  $[\text{Pt}(\text{tpy})\text{Cl}](\text{PF}_6)$  [28,29]. If the filtrate remains yellow, some additional  $\text{NH}_4\text{PF}_6$  should be added to use the remaining  $\text{Pt}(\text{tpy})\text{Cl}_2$ .

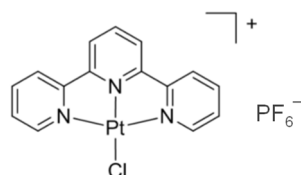
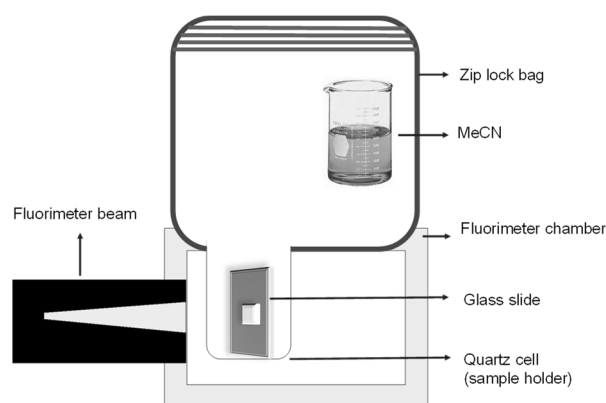


**Figure 1.** The chemical structure of the  $[\text{Pt}(\text{tpy})\text{Cl}](\text{PF}_6)$  [11].

Long, yellow crystalline needles of  $[\text{Pt}(\text{tpy})\text{Cl}](\text{PF}_6)$  are readily obtained through the evaporation of a 1:1 acetone/water mixture at room temperature. Subsequently, the crystals in the remaining water should be filtered using filter paper and a gravity funnel.

#### 2.4. Vapochromic Studies of $[\text{Pt}(\text{tpy})\text{Cl}](\text{PF}_6)$ Crystals

To record fluorescence spectra, the crystals of  $[\text{Pt}(\text{tpy})\text{Cl}](\text{PF}_6)$  were placed on a microscope slide with a layer of grease. Fluorescence detection was achieved by placing the crystals at a right angle in front of the photon beam. Samples were exposed to air saturated with MeCN at room temperature using a sealed plastic chamber ( $\sim 1.0$  L) with a MeCN solvent reservoir (Scheme 1) to initiate the MeCN vapor absorption process. Subsequently, the MeCN reservoir was removed, and the desorption process was monitored by recording the fluorescence spectra. The absorption and desorption of the MeCN onto and from  $[\text{Pt}(\text{tpy})\text{Cl}](\text{PF}_6)$  crystals were tracked by recording the fluorescence spectra at each step. The excitation wavelength ( $\lambda_{\text{ex}}$ ) was 436 nm. The experiments were conducted at room temperature ( $25^\circ\text{C}$ ) and atmospheric pressure, where the vapor pressure of MeCN was 0.117 atm [29].



**Scheme 1.** Instrumental set up for the fluorescence study of absorption and desorption of acetonitrile onto and from  $[\text{Pt}(\text{tpy})\text{Cl}](\text{PF}_6)$  crystals.

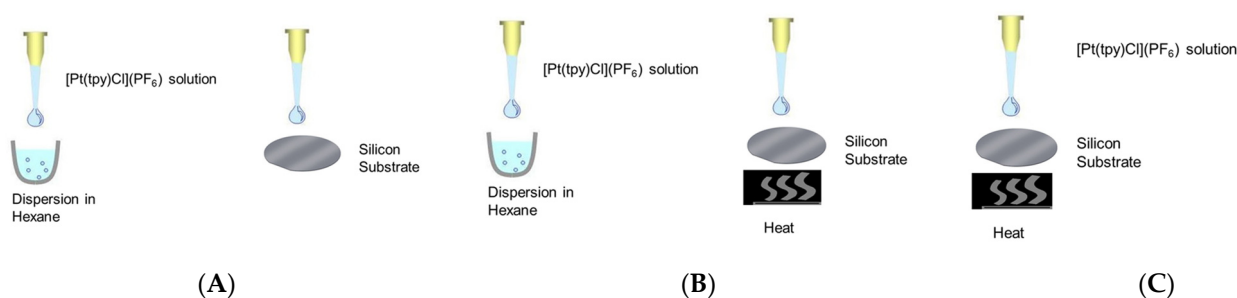
#### 2.5. Synthesis of $[\text{Pt}(\text{tpy})\text{Cl}]\text{PF}_6$ Nanocrystals

A total of 0.1 g of  $[\text{Pt}(\text{tpy})\text{Cl}](\text{PF}_6)$  powder was dissolved in a mixture of acetone and water (95:5 v/v) in a 10 mL volumetric flask. A silicon surface, previously cleaned in acetone and distilled water using ultrasound, was employed as a substrate. Using a micro syringe, 1.0  $\mu\text{L}$  of complex solution was dispensed onto the silicon surface.

To investigate the effect of dispersion and heat on the size of  $[\text{Pt}(\text{tpy})\text{Cl}](\text{PF}_6)$  nanocrystals, three different methods were employed, and scanning electron microscopic (SEM) images were subsequently examined:

In Methods 1 and 2: a single drop of a solution containing  $[\text{Pt}(\text{tpy})\text{Cl}](\text{PF}_6)$  at a concentration of  $1.6 \times 10^{-3} \text{ mol L}^{-1}$  in a mixture of acetone and water (95:5, *v/v*) was added to three drops of hexane (solution A).

Method #1. Subsequently,  $1.0 \mu\text{L}$  of solution A was applied onto the silicon substrate using a syringe (Scheme 2A).



**Scheme 2.** Synthesis of  $[\text{Pt}(\text{tpy})\text{Cl}](\text{PF}_6)$  nanocrystals using  $[\text{Pt}(\text{tpy})\text{Cl}](\text{PF}_6)$  at a concentration of  $1.6 \times 10^{-3} \text{ mol L}^{-1}$  in a mixture of acetone and water (95:5, *v/v*). (A) Method #1: dispersion of the  $[\text{Pt}(\text{tpy})\text{Cl}](\text{PF}_6)$  solution in hexane, followed by deposition onto a silicon substrate. (B) Method #2: dispersion of the  $[\text{Pt}(\text{tpy})\text{Cl}](\text{PF}_6)$  solution in hexane, followed by deposition onto a preheated silicon substrate. (C) Method #3: deposition of the  $[\text{Pt}(\text{tpy})\text{Cl}](\text{PF}_6)$  solution onto a preheated silicon substrate.

Method #2. Using a syringe,  $1.0 \mu\text{L}$  of solution A was dispensed onto a silicon substrate preheated for 5 min in an oven at  $105^\circ\text{C}$  (Scheme 2B).

Method #3. A total of  $1.0 \mu\text{L}$  of  $1.6 \times 10^{-3} \text{ mol L}^{-1}$   $[\text{Pt}(\text{tpy})\text{Cl}](\text{PF}_6)$  solution in an acetone and water mixture (95:5, *v/v*) was poured onto the preheated silicon substrate using a syringe directly (Scheme 2C). The silicon substrate was preheated for 5 min in an oven at  $105^\circ\text{C}$  to facilitate rapid solvent evaporation.

To investigate the type of substrate on  $[\text{Pt}(\text{tpy})\text{Cl}](\text{PF}_6)$  nanocrystal structures, the following procedure was implemented: First, 0.1 g of  $[\text{Pt}(\text{tpy})\text{Cl}](\text{PF}_6)$  was dissolved in a mixture of acetone and water (95:5, *v/v*) in a 10.0 mL volumetric flask. Then,  $1.0 \mu\text{L}$  of the solution was dropped onto either a silicon or glass slide substrates, preheated in the oven ( $105^\circ\text{C}$ ) for 5 min. Then, SEM images were examined.

To study the effect of  $[\text{Pt}(\text{tpy})\text{Cl}](\text{PF}_6)$  stock solution concentration on nanocrystal structures, the following procedure was performed: First, 0.02 g, 0.01 g, and 0.005 g of  $[\text{Pt}(\text{tpy})\text{Cl}](\text{PF}_6)$  were individually dissolved in 10 mL of acetone/water mixture (95:5, *v/v*) to produce  $3.2 \times 10^{-3}$ ,  $1.6 \times 10^{-3}$ , and  $0.8 \times 10^{-3} \text{ mol L}^{-1}$  stock solutions, respectively. Then,  $1.0 \mu\text{L}$  of each solution was dispensed onto the preheated silicon substrate (using Method 3) to fabricate nanocrystals. Subsequently, SEM images were studied.

## 2.6. Vapochromic Studies of $[\text{Pt}(\text{tpy})\text{Cl}](\text{PF}_6)$ Nanocrystals

A  $3.2 \times 10^{-3} \text{ mol L}^{-1}$   $[\text{Pt}(\text{tpy})\text{Cl}](\text{PF}_6)$  solution (saturated solution) was prepared using a mixture of acetone/water (95:5 *v/v*) in a 10.0 mL volumetric flask. A total of  $1.0 \mu\text{L}$  of the solution was dispensed onto a preheated silicon substrate at  $105^\circ\text{C}$ . The silicon, held on a glass slide, was positioned in front of the fluorimeter light source. The exposure to MeCN vapor was conducted at room temperature using a sealed plastic chamber with a MeCN solvent reservoir (Scheme 1). The absorption and desorption processes of MeCN onto and from the  $[\text{Pt}(\text{tpy})\text{Cl}](\text{PF}_6)$  nanocrystals were monitored by recording the fluorescence spectra for five cycles. The excitation wavelength ( $\lambda_{\text{ex}}$ ) was 436 nm. The experiments were conducted at room temperature ( $25^\circ\text{C}$ ) and atmospheric pressure, where the vapor pressure of MeCN was to be 0.117 atm [29].



### 3. Results and Discussion

#### 3.1. Characterization of $[Pt(tpy)Cl](PF_6)$ Crystals by $^1H$ NMR

The  $^1H$ NMR spectra of  $[Pt(tpy)Cl](PF_6)$  were taken at room temperature to confirm the synthesis of the compound. Chemical shifts were compared with the solvent (Figure 2). Each peak in the NMR spectrum represented a hydrogen in the structure, as shown in the figure. Therefore, the spectra could be analyzed separately as a four-spin system for the protons of the terminal rings (protons 1, 2, 3, and 4, along with their symmetry-related protons) and as an independent three-spin system for the protons of the central ring (protons 5, 6, and the symmetry-related proton of 5). The chemical shifts corresponding to the protons of terpyridine appeared at approximately 7.9 ppm for protons 2 and 2', 8.5 ppm for protons 3 and 3', 8.6 ppm for protons 5, 6, 5', 4, and 4', and 8.9 ppm for protons 1 and 1'. The peak at 3.3 ppm was attributed to water, and the peak at 2.5 ppm was attributed to dimethyl sulfoxide (DMSO), which was used to dissolve the crystals of  $[Pt(tpy)Cl](PF_6)$ .

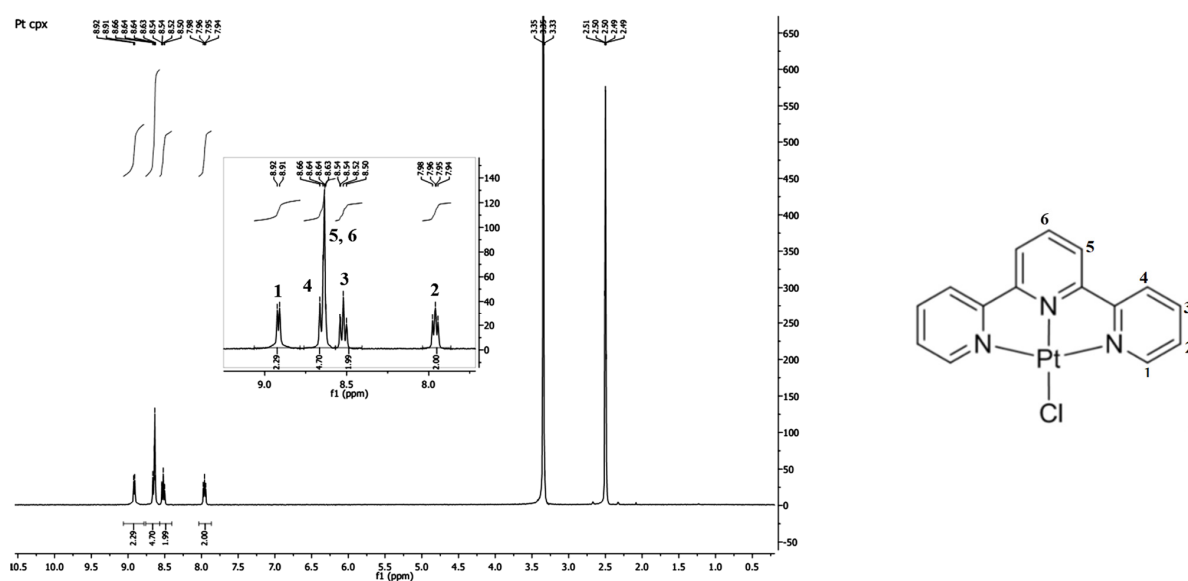


**Figure 2.** Characterization of  $[Pt(tpy)Cl](PF_6)$  crystals by  $^1H$ NMR.

#### 3.2. Characterization of $[Pt(tpy)Cl](PF_6)$ Crystals by X-ray Powder Diffraction

The crystallinity of  $[Pt(tpy)Cl](PF_6)$  was investigated by powder XRD in comparison with the simulated powder pattern from Mercury software (version 3.7) [30] by using the following parameters including temperature: 298.0 K; Start  $2\theta$ : 0 degree; End  $2\theta$ : 10 degree;  $2\theta$  step: 0.002 degree; calibration wavelength: 0.41362; FWHM: 0.05; and h, k, l: 0, 0, 1. The X-ray powder diffractograms are presented in Figure 3. Both diffractograms have the same pattern and characteristic diffraction peaks at  $2\theta$  degrees, confirming the formation and purity of  $[Pt(tpy)Cl](PF_6)$  crystals [30].

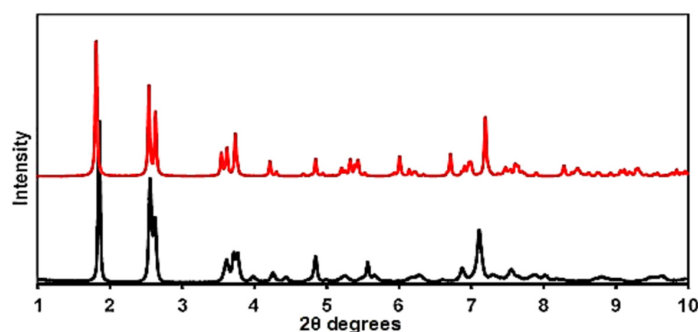


**Figure 3.** The X-ray powder diffractogram of the  $[Pt(tpy)Cl](PF_6)$  crystals (—) and the simulated pattern from the mercury software (—) [30].

### 3.3. Vapochromic Studies of the $[\text{Pt}(\text{tpy})\text{Cl}](\text{PF}_6)$ Crystals

#### 3.3.1. Studying Absorption/Desorption Cycle of MeCN Vapor in the Structure of $[\text{Pt}(\text{tpy})\text{Cl}](\text{PF}_6)$ Crystals

Figure 4A displays the fluorescence spectra of  $[\text{Pt}(\text{tpy})\text{Cl}](\text{PF}_6)$  ( $\lambda_{\text{ex}} = 436$  nm) crystals before and after exposure to MeCN vapors. When excited at 436 nm, the crystals show a consistent broad fluorescence band centered at 550 nm, which indicates high-quality crystals of  $[\text{Pt}(\text{tpy})\text{Cl}](\text{PF}_6)$ . After exposure to MeCN vapor in a sealed chamber (Scheme 1), the fluorescence spectrum broadens further, with a peak at 680 nm and a shoulder around 600–610 nm (Figure 4A), indicating the formation of an intermediate structure. This red shift suggests an increase in Pt...Pt interactions. To assess the fluorescence changes during the desorption, spectra were collected after exposing  $[\text{Pt}(\text{tpy})\text{Cl}](\text{PF}_6)$  crystals to MeCN vapors and then removing the MeCN source. The peak at 680 nm decreased while the peak at 600 nm increased (Figure 4B). The final fluorescence spectrum post-desorption differed from the initial one, suggesting that the original high-quality crystals could not be restored after MeCN desorption. The increased fluorescence intensity at 600 nm suggests the formation of solvated  $[\text{Pt}(\text{tpy})\text{Cl}](\text{PF}_6)$ , consistent with the absorption fluorescence spectra. When was exposed to MeCN vapors, the room-temperature fluorescence spectrum ( $\lambda_{\text{ex}} = 436$  nm) showed a broad band at 685 nm, attributed to the primary spin-forbidden metal–metal-to-ligand-charge transfer (MMLCT) transition [10,31]. The blue shift to 600 nm indicated that MeCN vapor desorption led to an increased Pt...Pt distance, weakening these interactions and destabilizing MMLCT states [10,31]. The 600 nm fluorescence band might be linked to MMLCT from Pt...Pt dimers, while the 685 nm fluorescence band in MeCN-vapor-exposed crystals was associated with MMLCT from a linear chain of closely interacting Pt centers [10,31]. In more detail, in the yellow crystals, the  $\text{d}_{z^2}$  orbitals are further apart, but in the red form, they are closer, as shown in Scheme 3. This closer distance boosts orbital interaction, forming  $\text{d}\sigma$  and  $\text{d}\sigma^*$  orbitals. The higher energy of the  $\text{d}\sigma^*$  orbital allows easier electron transfer to ligand  $\pi^*$  orbitals, causing a red shift in fluorescence. Thus, yellow crystals exhibit metal-to-ligand charge transfer (MLCT), while MeCN-exposed red crystals display MMLCT [10,31]. These interaction changes, combined with alterations in crystal morphology due to MeCN exposure, result in asymmetrical behavior in absorption/desorption fluorescence spectra. Previous studies have examined single-crystal XRD measurements of  $[\text{Pt}(\text{tpy})\text{Cl}](\text{PF}_6)$  crystals and MeCN-exposed ones [10].

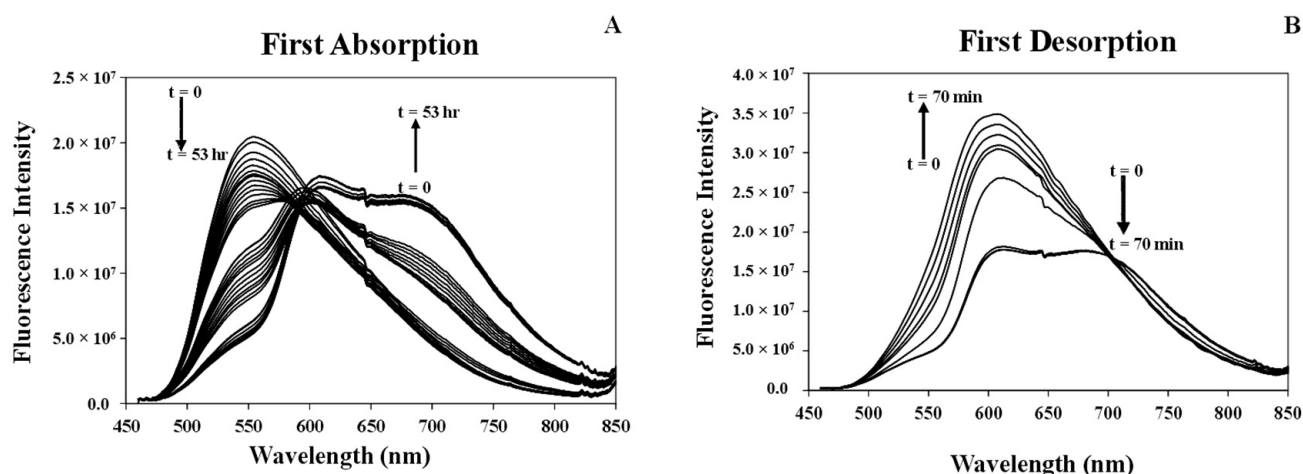
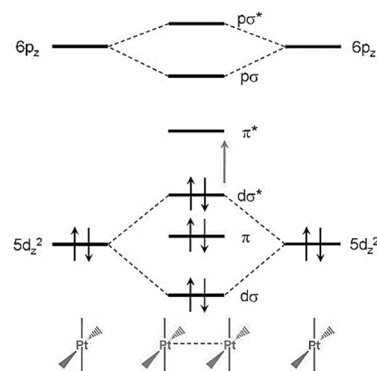


**Figure 4.** Fluorescence spectra of the crystals of Pt(II) complexes (by time) during the first absorption (A) and desorption (B) of acetonitrile vapor ( $\lambda_{\text{ex}} = 436$  nm).



**Scheme 3.** The interaction of Pt-Pt orbitals to form  $d\sigma$  and  $d\sigma^*$  orbitals and the possibility of MMLCT [10,31]. In detail, the closer distance of the  $d_z^2$  orbitals in MeCN-vapor-exposed crystals produces  $d\sigma$  and  $d\sigma^*$  orbitals. The higher energy of the  $d\sigma^*$  orbital allows easier electron transfer to ligand  $\pi^*$  orbitals.

The process of absorption/desorption cycling of MeCN vapors in  $[\text{Pt}(\text{tpy})\text{Cl}](\text{PF}_6)$  crystals was repeated multiple times. In the second cycle (Figure 5A,B), the maximum wavelength of the fluorescence shifted to 700 nm during MeCN absorption and then to 600 nm during desorption. Repeating the cycles five times showed that the maximum absorption peak remained at 700 nm (Figure 5C,E,G), while the desorption peak stayed at 600 nm (Figure 5D,F,H), consistent with the peaks in the second absorption/desorption cycle. It is worth noting that the peaks' intensity during the absorption and desorption cycles is significant enough to confidently suggest this crystal as a sensor for MeCN vapors.

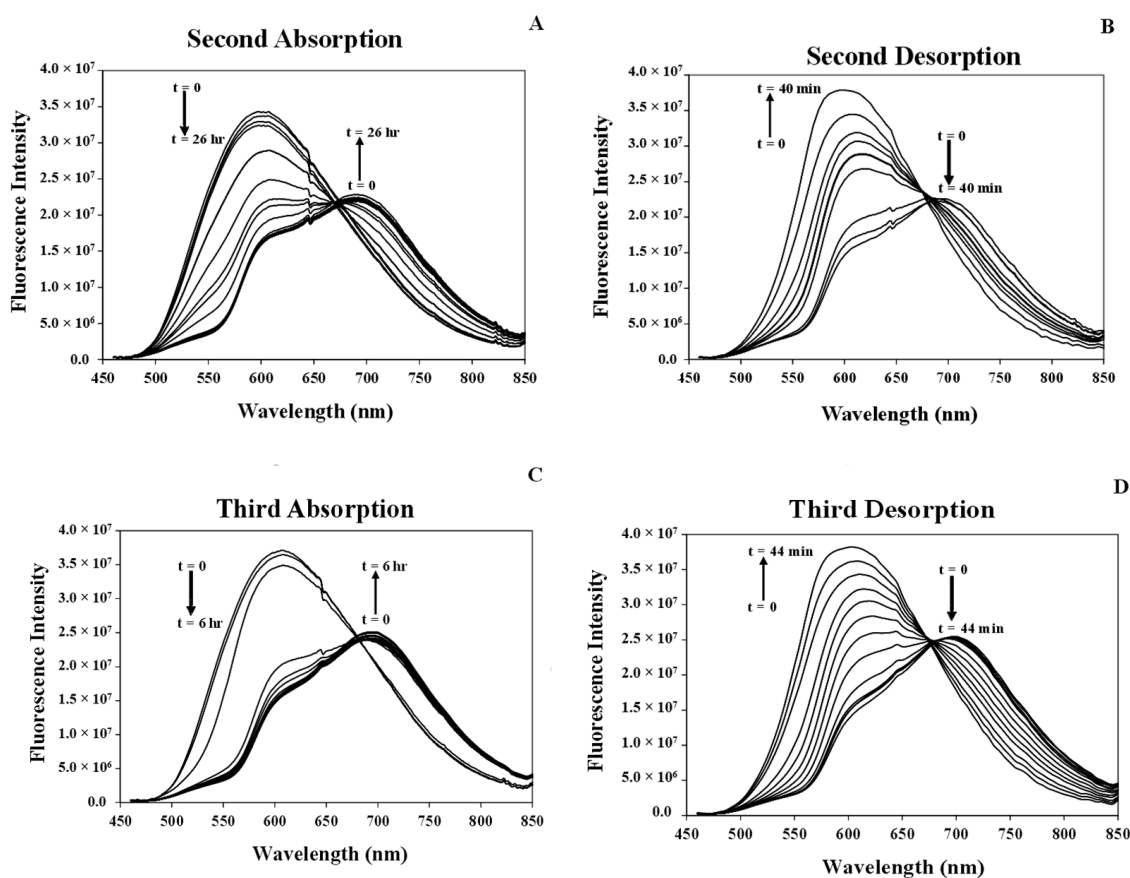


**Figure 5.** Cont.

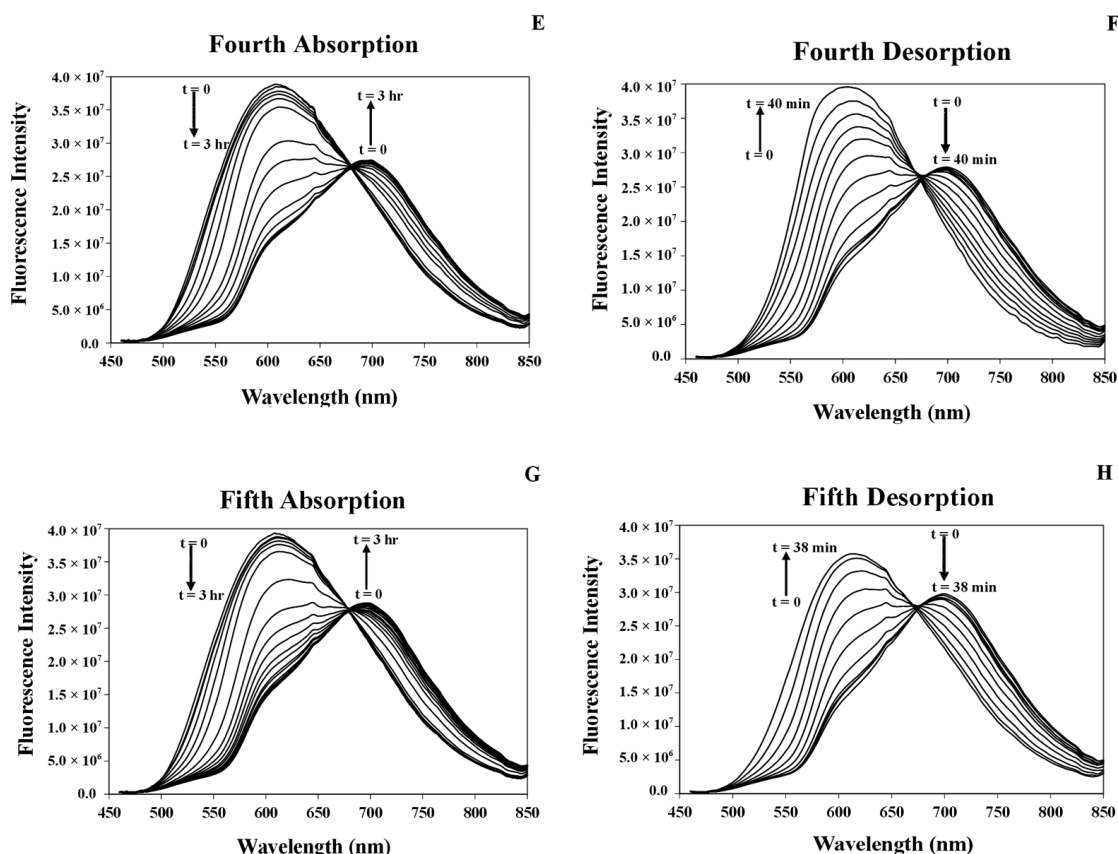


**Figure 5.** Fluorescence spectra of the crystals of Pt(II) complexes (by time) during the second (A,B), third (C,D), fourth (E,F), and fifth (G,H) absorption and desorption of acetonitrile vapor ( $\lambda_{\text{ex}} = 436 \text{ nm}$ ).

### 3.3.2. Vapochromic Studies on the Microscopic and SEM Images of the [Pt(tpy)Cl](PF<sub>6</sub>) Crystals before and after Being Exposed to MeCN Vapor

Long, yellow crystalline needles of [Pt(tpy)Cl](PF<sub>6</sub>) were grown by evaporating a solution of [Pt(tpy)Cl](PF<sub>6</sub>) in a 1:1 acetone/water mixture at room temperature. The crystals were then filtered using a gravity funnel and filter paper to obtain high quality crystals. It is crucial to avoid using a vacuum funnel, as it can create defects in the crystal structure. SEM images of the crystals are shown in Figure 6A–D, with different magnifications at (A) 100  $\mu\text{m}$ , (B) 20  $\mu\text{m}$ , (C) 20  $\mu\text{m}$ , and (D) 10  $\mu\text{m}$  scales, indicating that the crystals are defect-free. Microscopic images of these high-quality yellow crystals are presented in Figure 7A. When exposed to MeCN vapor, the color changes from yellow to red (Figure 7B) due to alterations in Pt . . . Pt interactions. Figure 8 shows SEM images of the crystals after the first (A), second (B), and fifth (C) absorption/desorption cycle of MeCN vapor. After the fifth cycle, changes in the crystal structure are evident. Cracks and defects begin to appear along the edges of the crystal (Figure 8A). These eventually cover most of the crystal surface and penetrate deep into the lattice structure (Figure 8B). During desorption, noticeable color changes from red to yellow spread from the crystal's long edge, resulting in a yellow crystal with visible defects. The accumulated observations suggest that stress from vapor absorption and desorption leads to fracturing and the formation of defects, resulting in a loss of long-range order, as seen in Figure 8C. Previous XRD and single-crystal XRD data for [Pt(tpy)Cl](PF<sub>6</sub>) and MeCN-exposed [Pt(tpy)Cl](PF<sub>6</sub>) were collected to confirm changes in Pt . . . Pt distances upon vapor absorption/desorption [10].



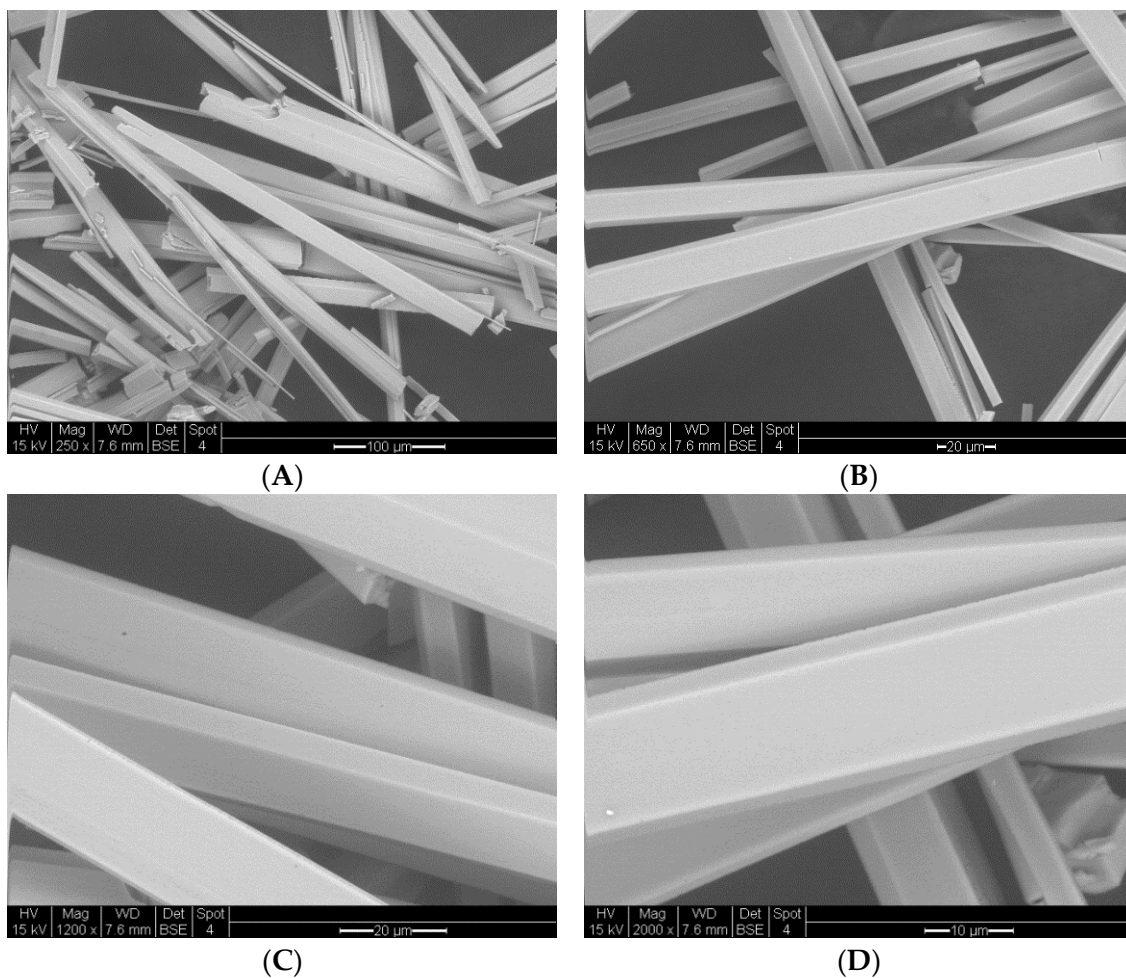


**Figure 6.** The SEM images of the high-quality [Pt(tpy)Cl](PF<sub>6</sub>) crystals with different magnifications: (A) 100  $\mu\text{m}$ , (B) 20  $\mu\text{m}$ , (C) 20  $\mu\text{m}$ , and (D) 10  $\mu\text{m}$ .

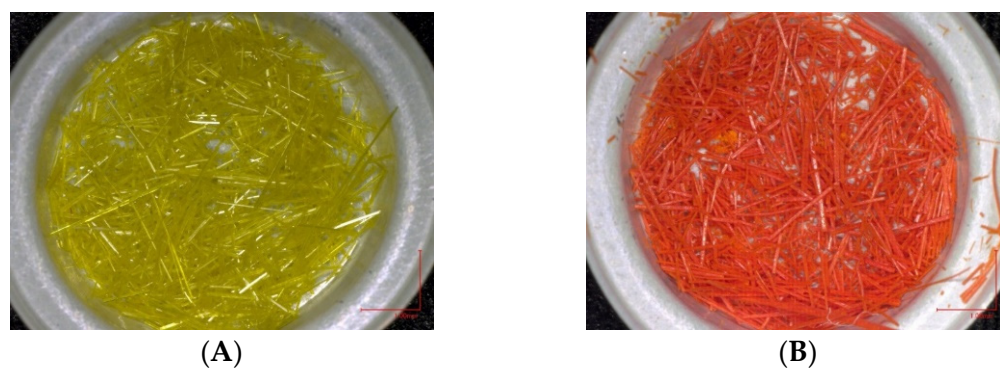


**Figure 7.** The microscopic images of [Pt(tpy)Cl](PF<sub>6</sub>) crystals' color change (A) before and (B) after exposure to MeCN vapor.



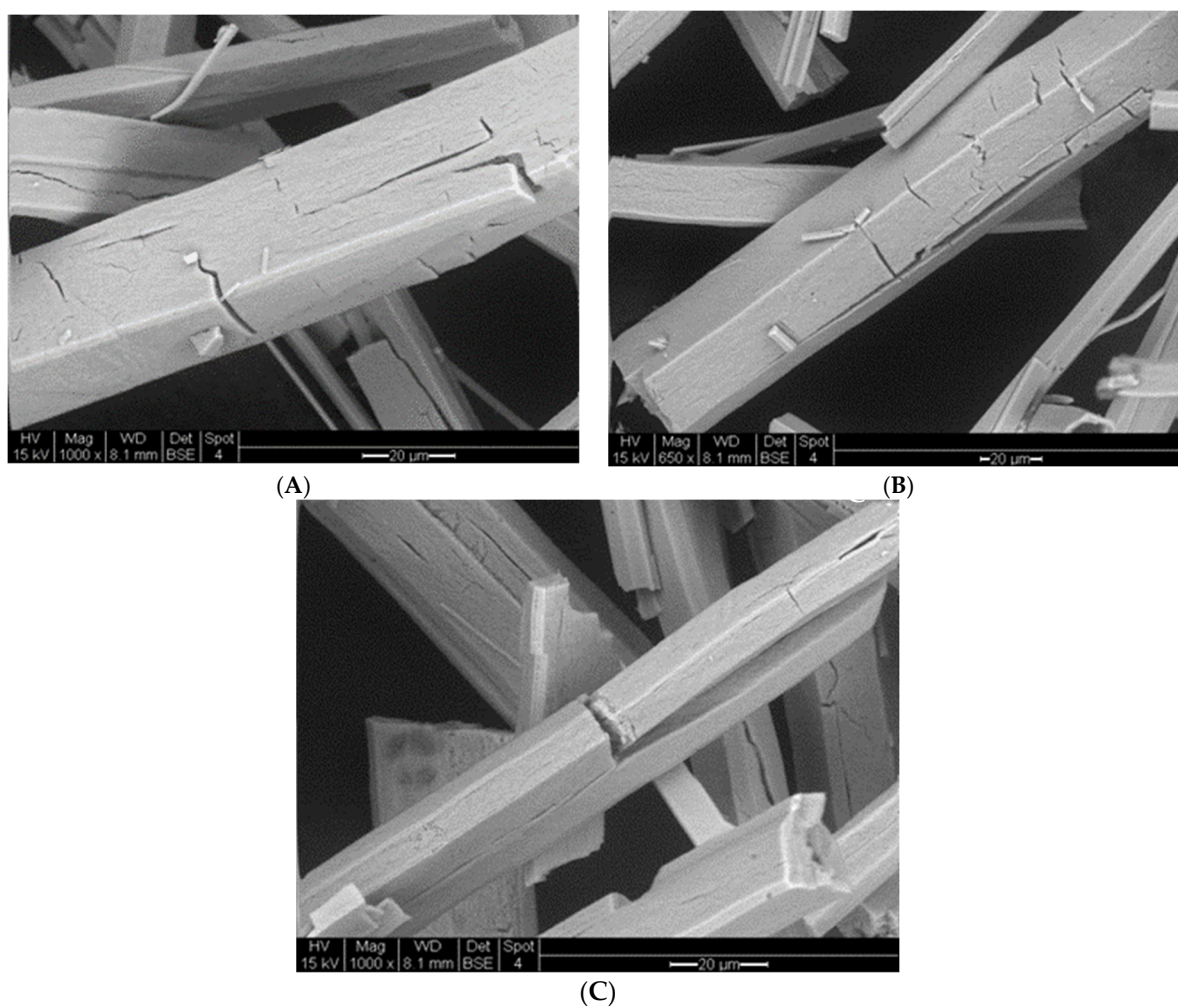


**Figure 8.** The SEM images of the  $[\text{Pt}(\text{tpy})\text{Cl}](\text{PF}_6)$  crystals after (A) first, (B) second, and (C) fifth absorption/desorption of MeCN vapor.

### 3.4. Characterization of $[\text{Pt}(\text{tpy})\text{Cl}](\text{PF}_6)$ Nanocrystals by Mass Spectroscopy

The nanocrystals formed on the silicon substrate were rinsed with MeCN and used for mass spectroscopic analysis. The  $[\text{Pt}(\text{tpy})\text{Cl}](\text{PF}_6)$  complex weighed 12.0  $\mu\text{g}$ , and the MeCN volume was 50.0  $\mu\text{L}$ . Using mass spectrometry–electrospray ionization (MS-ESI) in positive ion mode, MeCN ( $\text{CH}_3\text{CN}$ ) showed an  $m/z$  of 463.0 for  $[\text{Pt}(\text{tpy})\text{Cl}]^+$ . In the negative ion mode, MS-ESI showed an  $m/z$  of 144.9 for  $\text{PF}_6^-$ . Notably, the instrument was calibrated in positive ion mode using poly-alanine and in negative ion mode using sodium iodide. The observed isotope patterns closely matched those predicted based on natural isotopic abundances.

### 3.5. Investigation of the Effect of Dispersion and Heat on $[\text{Pt}(\text{tpy})\text{Cl}](\text{PF}_6)$ Nanocrystal Sizes

The SEM images of the samples prepared using three methods (described in Section 2.5) are displayed in Figure 9, with the corresponding width, length, and aspect ratio provided in Table 1. In Figure 9A, nanocrystals created by dispersing the  $[\text{Pt}(\text{tpy})\text{Cl}](\text{PF}_6)$  solution in hexane exhibited a large width of 170 nm, length of 3960 nm, and an aspect ratio of 26.1 owing to nanocrystal aggregation. This aggregation is attributed to the slow evaporation of the solvent in the presence of hexane on a cold silicon substrate. Figure 9B shows structures formed by first dispersing the solution in hexane and then pouring it onto a preheated silicon substrate. These nanocrystals had the smallest widths of 22 nm, lengths of 101.3 nm, and the lowest aspect ratio of 4.5. This likely occurred due to acetone's higher volatility compared to hexane, resulting in the formation of partially needle-shaped nanocrystals and partial

evaporation over extended periods, hindering nanocrystal formation. Evaporating the solution on a silicon substrate preheated in the oven, without initial dispersion in hexane, resulted in nanocrystals with widths of 89 nm, lengths of 2519 nm, and a high aspect ratio of 26.4, as shown in Figure 9C. This method generated more nanocrystals with reduced size and less aggregation compared to those produced by Methods 1 and 2, without requiring dispersion in hexane. This phenomenon is likely due to the miscibility of acetone and water, as well as the volatility of acetone compared to hexane.

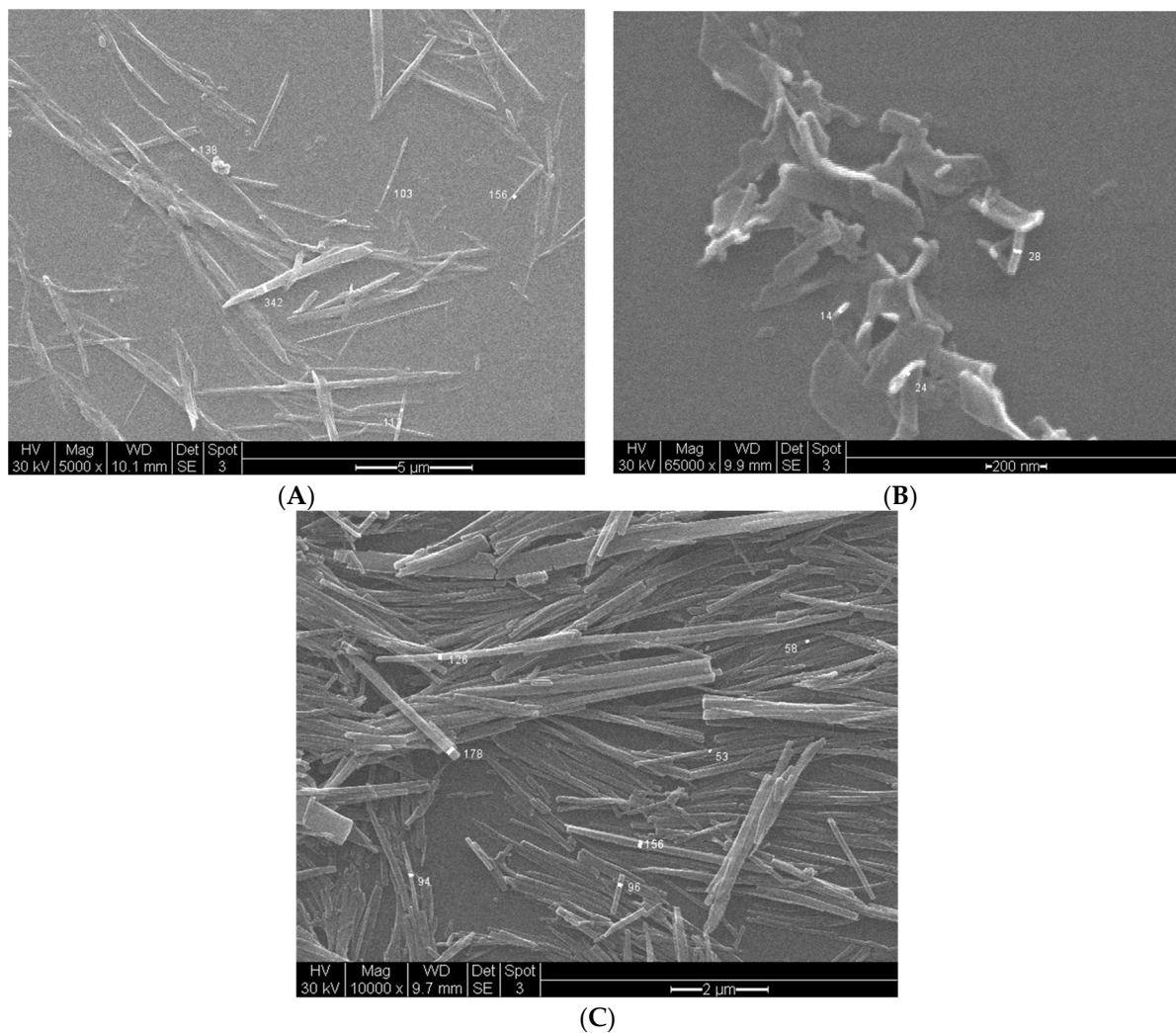


**Figure 9.** The SEM images of the  $[\text{Pt}(\text{tpy})\text{Cl}](\text{PF}_6)$  nanocrystals synthesized under different preparation conditions: (A) Method 1: Deposition of dispersed  $[\text{Pt}(\text{tpy})\text{Cl}](\text{PF}_6)$  onto a silicon substrate, (B) Method 2: Deposition of dispersed  $[\text{Pt}(\text{tpy})\text{Cl}](\text{PF}_6)$  onto a preheated silicon substrate, (C) Method 3: Direct deposition of  $[\text{Pt}(\text{tpy})\text{Cl}](\text{PF}_6)$  onto a preheated silicon substrate.

**Table 1.** The width, length, and aspect ratio of  $[\text{Pt}(\text{tpy})\text{Cl}](\text{PF}_6)$  nanocrystals generated using  $1.6 \times 10^{-3} \text{ mol L}^{-1}$   $[\text{Pt}(\text{tpy})\text{Cl}](\text{PF}_6)$  solution by various methods.

Method	Mean Width (nm) ( <i>n</i> = 10)	Mean Length (nm) ( <i>n</i> = 10)	Mean Aspect Ratio ( <i>n</i> = 10)
1 <sup>a</sup>	170.0	3960.0	26.1
2 <sup>b</sup>	22.0	101.3	4.5
3 <sup>c</sup>	89.0	2519.0	26.4

<sup>a</sup> Method 1: Deposition of dispersed  $[\text{Pt}(\text{tpy})\text{Cl}](\text{PF}_6)$  onto a silicon substrate. <sup>b</sup> Method 2: Deposition of dispersed  $[\text{Pt}(\text{tpy})\text{Cl}](\text{PF}_6)$  onto a preheated silicon substrate. <sup>c</sup> Method 3: Direct deposition of  $[\text{Pt}(\text{tpy})\text{Cl}](\text{PF}_6)$  onto a preheated silicon substrate.

The SEM images and the energy-dispersive X-ray spectroscopy (EDX) analysis, presented in Figures 9 and 10, respectively, confirm the formation of nanocrystals of  $[\text{Pt}(\text{tpy})\text{Cl}](\text{PF}_6)$  and reveal the presence of the elements from the compound, including Pt, C, N, Cl, P, and F. The SEM images suggest that the size of  $[\text{Pt}(\text{tpy})\text{Cl}](\text{PF}_6)$  nanocrystals can be modulated by changing the preparation conditions. Generating nanocrystals by depositing  $1.0\ \mu\text{L}$  of  $1.6 \times 10^{-3}\ \text{mol L}^{-1}$   $[\text{Pt}(\text{tpy})\text{Cl}](\text{PF}_6)$  solution onto a preheated silicon substrate (for 5 min in an oven at  $105\ ^\circ\text{C}$ ) using a syringe (Method 3) resulted in satisfactory nanometer-sized nanocrystal widths with a high aspect ratio, which were selected for further experiments.

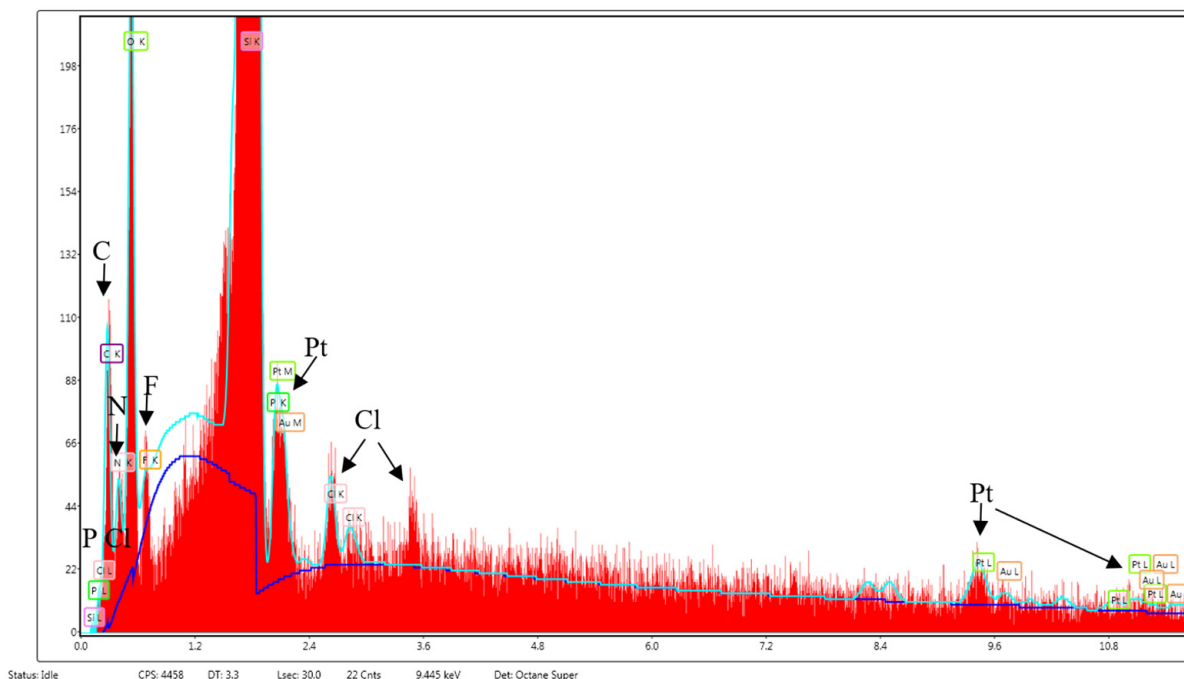


**Figure 10.** The EDX obtained from nanocrystals of  $[\text{Pt}(\text{tpy})\text{Cl}](\text{PF}_6)$ , which confirms the presence of the elements of the compound.

### 3.6. Effect of $[\text{Pt}(\text{tpy})\text{Cl}]\text{PF}_6$ Stock Solution Concentration on Nanocrystal Structures

The SEM images of the nanocrystals, produced by using various concentrations of  $[\text{Pt}(\text{tpy})\text{Cl}](\text{PF}_6)$  stock solutions, are depicted in Figure 11, illustrating the sizes and shapes of nanocrystals modulated by different solution concentrations. As shown in Figure 11A, nanocrystals formed from an  $8.0 \times 10^{-4}\ \text{mol L}^{-1}$   $[\text{Pt}(\text{tpy})\text{Cl}](\text{PF}_6)$  solution had a mean width of 83 nm, a mean length of 233 nm, and an aspect ratio of 3.6. In Figure 11B, nanocrystals from a  $1.6 \times 10^{-3}\ \text{mol L}^{-1}$  stock solution exhibited a mean width of 88 nm, a mean length of 209 nm, and an aspect ratio of 2.5. However, these structures appeared less uniform compared to the nanocrystals shown in Figure 11C, which originated from a  $3.2 \times 10^{-3}\ \text{mol L}^{-1}$  solution. The nanocrystals from this higher concentration displayed a mean width of 53 nm, a mean length of 951 nm, and an aspect ratio of 17.9. Notably, these nanocrystals not only exhibited uniformity but also narrower width and a satisfactory aspect ratio.



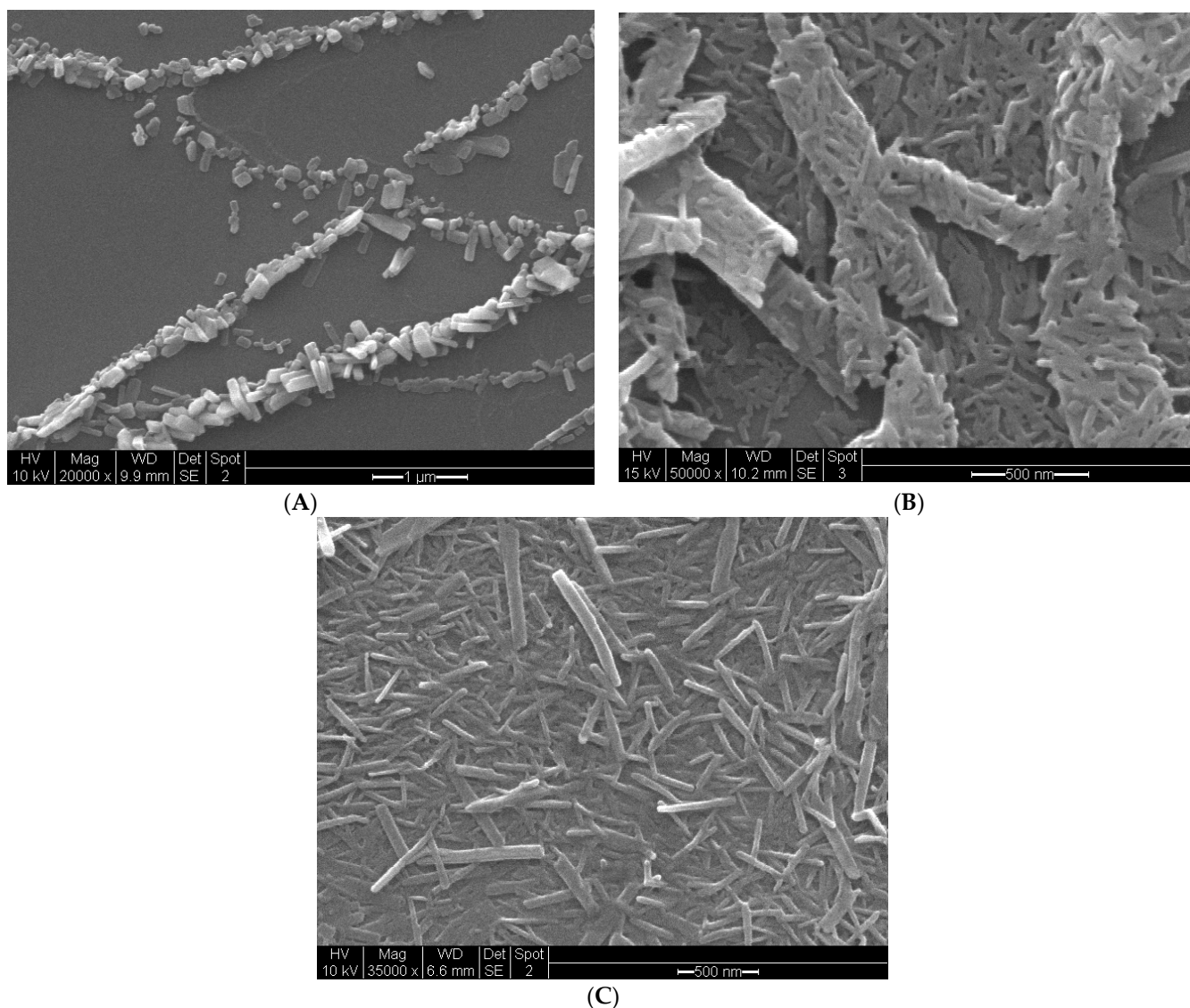


**Figure 11.** Effect of  $\text{Pt}[(\text{tpy})\text{Cl}]\text{PF}_6$  stock solution concentration ((A)  $8.0 \times 10^{-4} \text{ mol L}^{-1}$ , (B)  $1.6 \times 10^{-3} \text{ mol L}^{-1}$ , (C)  $3.2 \times 10^{-3} \text{ mol L}^{-1}$ ) on nanocrystal structures.

### 3.7. Vapochromic Studies of $[\text{Pt}(\text{tpy})\text{Cl}](\text{PF}_6)$ Nanocrystals

#### 3.7.1. Studying Absorption/Desorption of MeCN Vapor in the Structure of $[\text{Pt}(\text{tpy})\text{Cl}](\text{PF}_6)$ Nanocrystals

Figure 12 shows the fluorescence spectra of  $[\text{Pt}(\text{tpy})\text{Cl}](\text{PF}_6)$  nanocrystals ( $\lambda_{\text{ex}} = 436 \text{ nm}$ ) before and after exposure to MeCN vapor. Exciting the nanocrystals at 436 nm results in a consistent broad fluorescence band centered at 565 nm. Exposing the nanocrystal to MeCN vapor in a sealed chamber results in a slight decrease in intensity at 565 nm during initial MeCN absorption, but a red shift was observed from 565 to 585 nm. This exposure led to a broad fluorescence band with a maximum fluorescence at 715 nm and a shoulder near 580–585 nm (Figure 12A) due to the formation of an intermediate structure of solvated  $[\text{Pt}(\text{tpy})\text{Cl}](\text{PF}_6)$  nanocrystals. The red shift in the fluorescence band is consistent with an increase in Pt...Pt interactions [31]. During desorption, upon removal of the MeCN vapor source, a decrease in intensity at 715 nm and an increase in intensity at 585 nm were observed (Figure 12B). The intensity of the 585 nm fluorescence band rapidly increases over a period of 16 min, but the final fluorescence spectrum differed from that of the initial  $[\text{Pt}(\text{tpy})\text{Cl}](\text{PF}_6)$  nanocrystals, indicating that the initial nanocrystals could not be restored after desorption. The increased

intensity in the 585 nm shoulder with the loss of MeCN suggests that the short wavelength shoulder results from deformation of  $[\text{Pt}(\text{tpy})\text{Cl}](\text{PF}_6)$  nanocrystals.

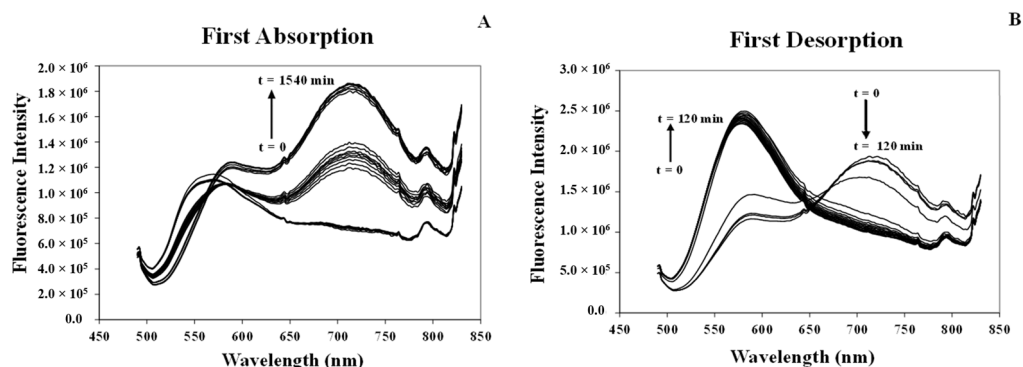


**Figure 12.** Fluorescence spectra of the nanocrystals of  $[\text{Pt}(\text{tpy})\text{Cl}](\text{PF}_6)$  (by time) during the first (A) absorption and (B) desorption of MeCN vapor ( $\lambda_{\text{ex}} = 436 \text{ nm}$ ).

At room temperature, the fluorescence spectrum ( $\lambda_{\text{ex}} = 436 \text{ nm}$ ) of  $[\text{Pt}(\text{tpy})\text{Cl}](\text{PF}_6)$  nanocrystals exhibited a broad band at 715 nm when exposed to MeCN vapor, preliminarily attributed to the primary spin-forbidden MMLCT transition of the lowest energy level [31]. The blue shift to 585 nm is consistent with MeCN desorption, causing an increase in the Pt...Pt distances, weakening these interactions and destabilizing MMLCT states [31]. The 585 nm fluorescence band was indecisively attributed to a MMLCT transition resulting from Pt...Pt dimers, whereas the 715 nm fluorescence band of the MeCN-exposed film was assigned to an MMLCT transition resulting from a linear chain of closely interacting Pt centers [31].

The process of absorbing and desorbing MeCN in the structure of  $[\text{Pt}(\text{tpy})\text{Cl}](\text{PF}_6)$  nanocrystals was repeated multiple times. In the second cycle (Figure 13A,B), it was observed that the maximum wavelength for the MeCN vapor absorption shifted to 720 nm and then to 585 nm during desorption. Repeating the cycles five times showed that the absorption peak remained at 720 nm (Figure 13C,E,G) while the desorption peak remained at 585 nm (Figure 13D,F,H), consistent with the second desorption peak. Importantly, the intensity of the peaks during the absorption and desorption cycles is sufficiently high to propose this compound as a sensor for MeCN vapor detection.

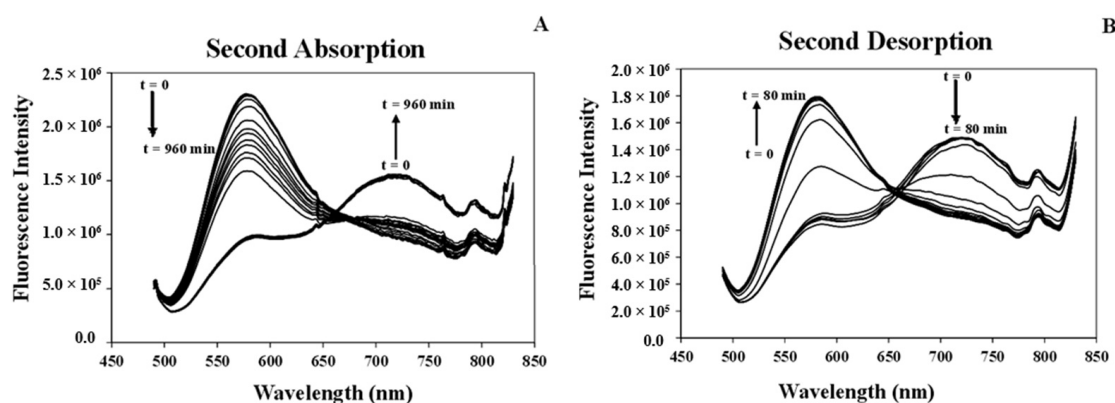


**Figure 13.** Cont.



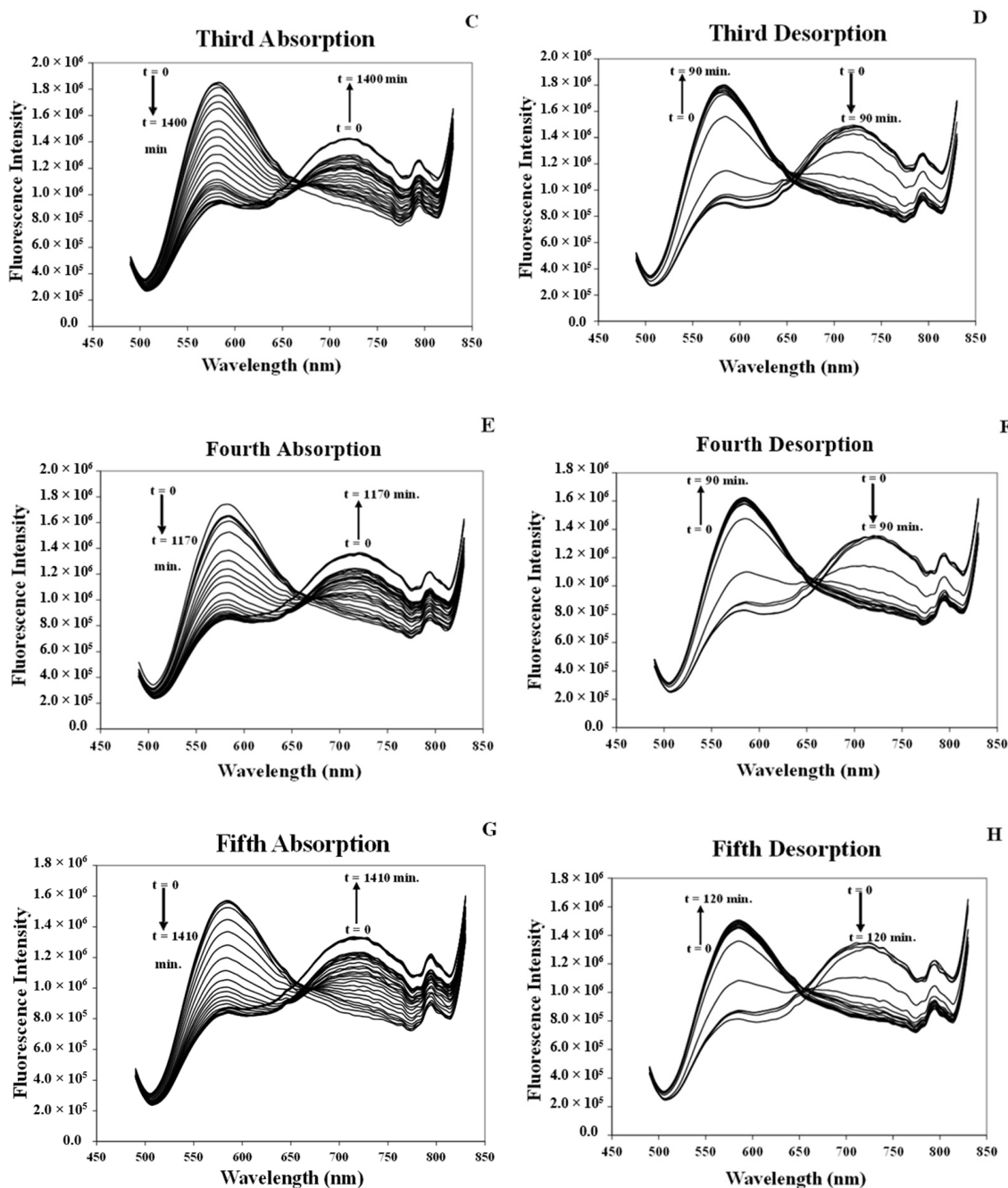
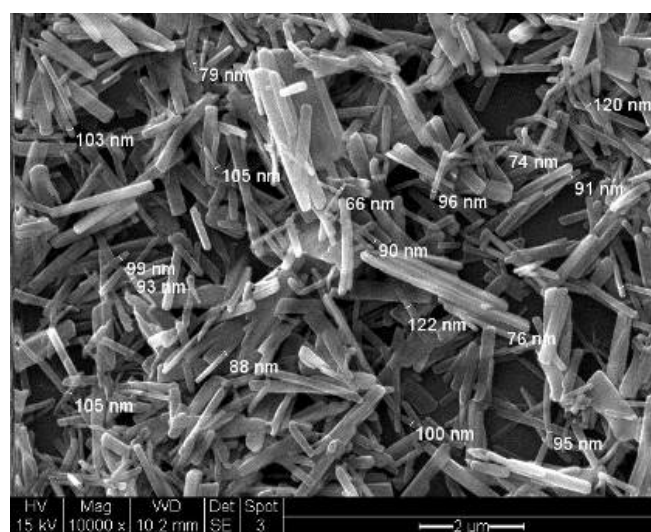


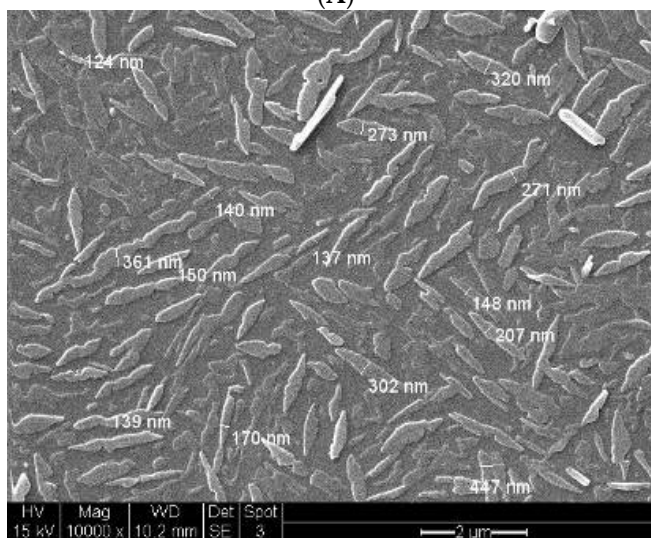
**Figure 13.** Fluorescence spectra of the nanocrystals of Pt(II) complexes (by time) during the second to fifth absorption (A,C,E,G) and desorption (B,D,F,H) of MeCN vapor ( $\lambda_{\text{ex}} = 436 \text{ nm}$ ).

### 3.7.2. Vapochromic Studies on the SEM Images of the [Pt(tpy)Cl](PF<sub>6</sub>) Nanocrystals before and after Being Exposed to MeCN Vapor

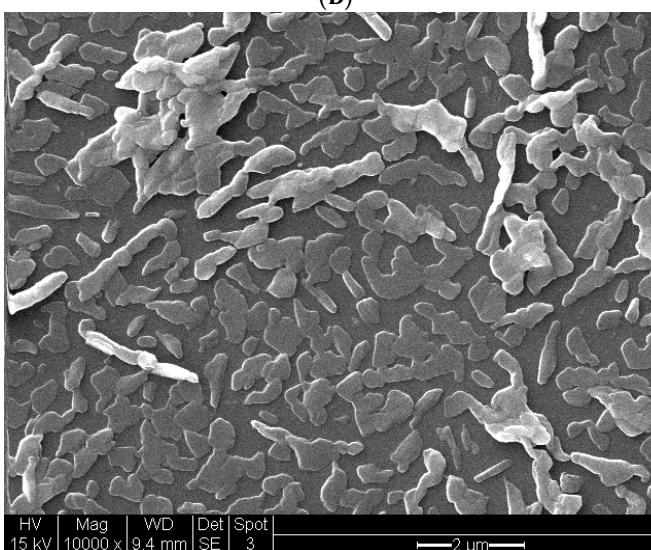
Initially, the [Pt(tpy)Cl](PF<sub>6</sub>) nanocrystals appear well-shaped, with each nanocrystal being individually distinguishable (See Figure 14). However, when exposed to MeCN vapor, the nanocrystals appear to be destroyed, deformed, and merged (Figure 14B). Additionally, SEM images of nanocrystals after five cycles of MeCN vapor absorption/desorption were recorded (Figure 14C), demonstrating significant changes in the nanocrystal structure. Unlike the crystals, there were no defects on the nanocrystal structures, but they had merged and lost their original shapes. These observations suggest that the stress associated with vapor absorption and desorption led to the malformation of nanocrystals, resulting in the loss of their nanosized structure.



(A)



(B)



(C)

**Figure 14.** The SEM images of  $[\text{Pt}(\text{tpy})\text{Cl}](\text{PF}_6)$  nanocrystals (A) before exposure to MeCN vapor (66–122 nm), (B) merged together (120–450 nm) after exposure to MeCN vapor, (C) after 5 cycles of MeCN vapor absorption/desorption.

### 3.7.3. Response Time of the [Pt(tpy)Cl](PF<sub>6</sub>) Nanocrystals for the Absorption/Desorption of MeCN Vapor

The fluorescence signal intensity of [Pt(tpy)Cl](PF<sub>6</sub>) nanocrystals during the MeCN vapor absorption over time was plotted. Figure 15 shows that during absorption, signal intensity decreased over time at  $\lambda = 585$  nm and increased at  $\lambda = 720$  nm. Hence, either of these wavelengths can be used to detect changes. Notably, during the first exposure cycle, there was no change in signal intensity at  $\lambda = 585$  nm, but changes in the first absorption process could be tracked at  $\lambda = 720$  nm. It is concluded from the response times that MeCN vapor absorption onto [Pt(tpy)Cl](PF<sub>6</sub>) nanocrystals resulted in signal changes within a period of less than 100 min.

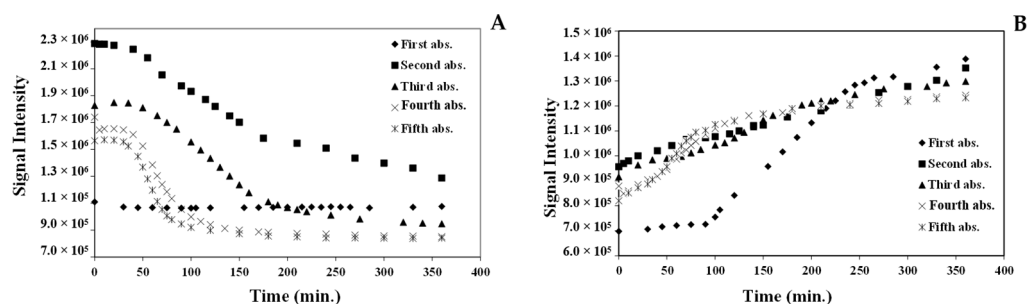


**Figure 15.** The [Pt(tpy)Cl](PF<sub>6</sub>) nanocrystals response time during MeCN vapor absorption at (A)  $\lambda = 585$  nm and (B)  $\lambda = 720$  nm.

Similarly, the fluorescence signal intensity of [Pt(tpy)Cl](PF<sub>6</sub>) nanocrystals during MeCN vapor desorption was recorded over time and plotted (Figure 16). It was observed that during desorption, the signal intensity decreased over time at  $\lambda = 720$  nm and increased at  $\lambda = 585$  nm. Hence, either of these wavelengths can be employed to detect changes. The response times confirmed MeCN vapor desorption from [Pt(tpy)Cl](PF<sub>6</sub>) nanocrystals occurred within a time period of less than 26 min.

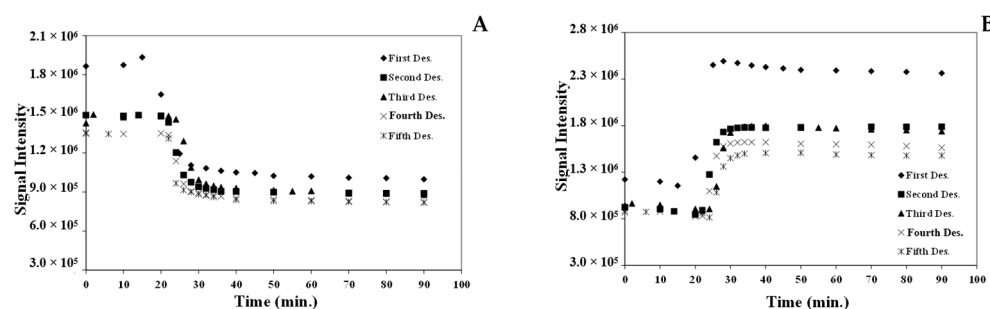


**Figure 16.** The [Pt(tpy)Cl](PF<sub>6</sub>) nanocrystals response time during MeCN vapor desorption at (A)  $\lambda = 720$  nm and (B)  $\lambda = 585$  nm.

### 3.8. Comparison of the Response Times of MeCN Vapor Absorption/Desorption of the [Pt(tpy)Cl](PF<sub>6</sub>) Crystals and Nanocrystals

The fluorescence-spectroscopy-monitored vapor absorption/desorption cycles, repeated several times, have demonstrated the reliability and effectiveness of these materials in real-world sensing applications. According to the data in Table 2, during the first cycle of MeCN vapor absorption, [Pt(tpy)Cl](PF<sub>6</sub>) nanocrystals indicated a response time of 100 min, compared to 11 h for [Pt(tpy)Cl](PF<sub>6</sub>) crystals. Subsequent cycles of MeCN vapor absorption showed a response time of 10 min for nanocrystals, compared to 9 h or 75 min for crystals, confirming that nanocrystals serve as superior sensors. Although crystal defects in later cycles contribute to faster responses to MeCN, the desorption time of MeCN vapor from nanocrystals and crystals remains almost the same except for the first desorption from crystals.

**Table 2.** Comparison of the response times to MeCN vapor absorption/desorption in the [Pt(tpy)Cl](PF<sub>6</sub>) crystals and nanocrystals in 5 cycles.

Cycles	Whole Absorption Time (h)		Absorption Response (min.)		Whole Desorption Time (min.)		Desorption Response (min.)	
	Crystal	Nanocrystal	Crystal (I700/I600)	Nanocrystal (I720/I585)	Crystal	Nanocrystal	Crystal (I600/I700)	Nanocrystal (I585/I720)
1	48	11.5	11 h	100	70	36	45	20
2	18	7.5	9 h	10	40	36	25	24
3	2	9.3	75	10	44	34	28	24
4	2	6.0	75	10	40	36	24	24
5	2	6.0	75	10	38	60	26	26

#### 4. Conclusions

This paper investigated the effects of various factors, including dispersion in hexane, temperature, and stock solution concentration, on the fabrication of [Pt(tpy)Cl](PF<sub>6</sub>) nanocrystals. Consequently, the fluorescence studies and SEM images confirmed that the [Pt(tpy)Cl](PF<sub>6</sub>) compound is vapochromic with nanosized dimensions as well. Finally, sensors constructed from [Pt(tpy)Cl](PF<sub>6</sub>) nanocrystals are expected to exhibit faster response times compared to bulk sensors in MeCN vapor absorption/desorption detection.

**Author Contributions:** Conceptualization: W.B.C.; formal analysis: S.B.; investigation: S.B. and M.K.A.; methodology: S.B. and M.K.A.; supervision: M.K.A. and G.A.; roles/writing—original draft and writing: S.B.; review and editing: G.A. and M.K.A. All authors have read and agreed to the published version of the manuscript.

**Funding:** This research was funded by the National Science Foundation (CHE-1152853).

**Data Availability Statement:** The original contributions presented in the study are included in the article, further inquiries can be directed to the corresponding author.

**Acknowledgments:** The authors wish to acknowledge the support of this work by Shiraz University Research Council.

**Conflicts of Interest:** The authors declare no conflict of interest.

#### References

- Kato, M.; Ito, H.; Hasegawa, M.; Ishii, K. Soft Crystals: Flexible Response Systems with High Structural Order. *Chem. A Eur. J.* **2019**, *25*, 5105–5112. [\[CrossRef\]](#)
- Evariste, S.; Khalil, A.M.; Kerneis, S.; Xu, C.; Calvez, G.; Costuas, K.; Lescop, C. Luminescent Vapochromic Single Crystal to Single Crystal Transition in One-Dimensional Coordination Polymer Featuring the First Cu(I) Dimer Bridged by an Aqua Ligand. *Inorg. Chem. Front.* **2020**, *7*, 3402–3411. [\[CrossRef\]](#)
- Utrera-Melero, R.; Huitorel, B.; Cordier, M.; Mevellec, J.-Y.; Massuyeau, F.; Latouche, C.; Martineau-Corcoss, C.; Perruchas, S. Combining Theory and Experiment to Get Insight into the Amorphous Phase of Luminescent Mechanochromic Copper Iodide Clusters. *Inorg. Chem.* **2020**, *59*, 13607–13620. [\[CrossRef\]](#)
- Sergeenko, A.S.; Ovens, J.S.; Leznoff, D.B. Copper(II) Dihalotetracyanoplatinate(IV) Coordination Polymers and Their Vapochromic Behavior. *Inorg. Chem.* **2017**, *56*, 7870–7881. [\[CrossRef\]](#)
- Karabacak, S.; Qun, D.L.C.; Ammanath, G.; Yeasmin, S.; Yagmurcukardes, M.; Alagappan, P.; Liedberg, B.; Yıldız, Ü.H. Polarity Induced Vapochromism and Vapoluminescence of Polythiophene Derivatives for Volatile Organic Compounds Classification. *Sens. Actuators B Chem.* **2023**, *389*, 133884. [\[CrossRef\]](#)
- Zhang, X.; Li, B.; Chen, Z.-H.; Chen, Z.-N. Luminescence Vapochromism in Solid Materials Based on Metal Complexes for Detection of Volatile Organic Compounds (VOCs). *J. Mater. Chem.* **2012**, *22*, 11427. [\[CrossRef\]](#)
- Yam, V.W.-W.; Au, V.K.-M.; Leung, S.Y.-L. Light-Emitting Self-Assembled Materials Based on D8 and D10 Transition Metal Complexes. *Chem. Rev.* **2015**, *115*, 7589–7728. [\[CrossRef\]](#)
- Li, E.; Jie, K.; Liu, M.; Sheng, X.; Zhu, W.; Huang, F. Vapochromic Crystals: Understanding Vapochromism from the Perspective of Crystal Engineering. *Chem. Soc. Rev.* **2020**, *49*, 1517–1544. [\[CrossRef\]](#)
- Taylor, S.D.; Howard, W.; Kaval, N.; Hart, R.; Krause, J.A.; Connick, W.B. Solid-State Materials for Anion Sensing in Aqueous Solution: Highly Selective Colorimetric and Luminescence-Based Detection of Perchlorate Using a Platinum(II) Salt. *Chem. Commun.* **2010**, *46*, 1070. [\[CrossRef\]](#)

10. Taylor, S. *Solid-State Structures and Electronic Properties of Platinum(II) Terpyridyl Complexes: Implications for Vapor and Aqueous Anion Sensing*; University of Cincinnati: Cincinnati, OH, USA, 2011.
11. Ni, J.; Zheng, W.; Qi, W.-J.; Guo, Z.-C.; Liu, S.-Q.; Zhang, J.-J. Synthesis, Structure and Luminescent Switching Properties of Cycloplatinated(II) Complexes Bearing Phenyl  $\beta$ -Diketone Ligands. *J. Organomet. Chem.* **2021**, *952*, 122048. [CrossRef]
12. Ohno, K.; Shiraishi, K.; Sugaya, T.; Nagasawa, A.; Fujihara, T. Cyclometalated Platinum(II) Complexes in a *Cis-N, N* Configuration: Photophysical Properties and Isomerization to Trans Isomers. *Inorg. Chem.* **2022**, *61*, 3420–3433. [CrossRef]
13. Li, B.; Liang, Z.; Yan, H.; Li, Y. Visual Self-Assembly and Stimuli-Responsive Materials Based on Recent Phosphorescent Platinum(II) Complexes. *Mol. Syst. Des. Eng.* **2020**, *5*, 1578–1605. [CrossRef]
14. Soto, M.A.; Kandel, R.; MacLachlan, M.J. Chromic Platinum Complexes Containing Multidentate Ligands. *Eur. J. Inorg. Chem.* **2021**, *2021*, 894–906. [CrossRef]
15. Shiotsuka, M.; Ono, R.; Kurono, Y.; Asano, T.; Sakae, Y. Photoluminescence of Platinum(II) Diethynylphenanthroline Organometallic Complexes with Bis-Arylethynyl Derivatives in Solution and Solid State. *J. Organomet. Chem.* **2019**, *880*, 116–123. [CrossRef]
16. Shiotsuka, M.; Asano, T.; Kurono, Y.; Ono, R.; Kawabe, R. Synthesis and Photophysical Characterization of Phosphorescent Platinum(II) Bis-(Trimethylsilyl)Ethynyl-Phenanthroline Organometallic Complexes with Bis-Arylethynyl Derivatives. *J. Organomet. Chem.* **2017**, *851*, 1–8. [CrossRef]
17. Shiotsuka, M.; Goto, A.; Miura, S.; Uekusa, H.; Ono, R. Vapochromism and Vapoluminescence of Platinum(II) 3,8-Bis-(3-Hydroxy-3-Methylbut-1-Yn-1-Yl)-Phenanthroline Organometallic Complexes with Bis-Arylethynyl Derivatives. *J. Organomet. Chem.* **2020**, *929*, 121554. [CrossRef]
18. Shiotsuka, M.; Ogihara, M.; Hanada, T.; Kasai, K. Multicolor Detection with Vapochromism of Platinum(II) 3,8-Bis-(2-Triethylsilylethynyl)-Phenanthroline Organometallic Complexes with Bis-Arylethynyl Derivatives. *J. Organomet. Chem.* **2022**, *965–966*, 122334. [CrossRef]
19. Norton, A.E.; Karimi Abdolmaleki, M.; Zhao, D.; Taylor, S.D.; Kennedy, S.R.; Ball, T.D.; Bovee, M.O.; Connick, W.B.; Chatterjee, S. Vapoluminescence Hysteresis in a Platinum(II) Salt-Based Humidity Sensor: Mapping the Vapochromic Response to Water Vapor. *Sens. Actuators B Chem.* **2022**, *359*, 131502. [CrossRef]
20. Ni, J.; Guo, Z.; Zhu, Q.; Liu, S.; Zhang, J. The Two-Stepwise Luminescent Switching Properties of Triple-Stimuli-Responsive Platinum(II) Complexes Bearing 4,4'-Bis(2-Phenylethynyl)-2,2'-Bipyridine Ligand. *Dye. Pigment.* **2023**, *217*, 111406. [CrossRef]
21. Kobayashi, A.; Kato, M. Vapochromic Platinum(II) Complexes: Crystal Engineering toward Intelligent Sensing Devices. *Eur. J. Inorg. Chem.* **2014**, *2014*, 4469–4483. [CrossRef]
22. Lai, S.-W.; Chan, M.C.W.; Cheung, K.-K.; Che, C.-M. Spectroscopic Properties of Luminescent Platinum(II) Complexes Containing 4,4',4''-Tri-Tert-Butyl-2,2':6',2''-Terpyridine ( $t\text{Bu}_3\text{Tpy}$ ). Crystal Structures of  $[\text{Pt}(t\text{Bu}_3\text{Tpy})\text{Cl}]\text{ClO}_4$  and  $[\text{Pt}(t\text{Bu}_3\text{Tpy})\{\text{CH}_2\text{C}(\text{O})\text{Me}\}]\text{ClO}_4$ . *Inorg. Chem.* **1999**, *38*, 4262–4267. [CrossRef]
23. Büchner, R.; Cunningham, C.T.; Field, J.S.; Haines, R.J.; McMillin, D.R.; Summerton, G.C. Luminescence Properties of Salts of the  $[\text{Pt}(4'\text{Ph-Terpy})\text{Cl}]^+$  Chromophore: Crystal Structure of the Red Form of  $[\text{Pt}(4'\text{Ph-Terpy})\text{Cl}]\text{BF}_4$  ( $4'\text{Ph-Terpy} = 4'\text{-Phenyl-2,2':6',2''-Terpyridine}$ ). *J. Chem. Soc. Dalton Trans.* **1999**, *999*, 711–718. [CrossRef]
24. Hill, M.G.; Bailey, J.A.; Miskowski, V.M.; Gray, H.B. Spectroelectrochemistry and Dimerization Equilibria of Chloro(Terpyridine)-Platinum(II). Nature of the Reduced Complexes. *Inorg. Chem.* **1996**, *35*, 4585–4590. [CrossRef]
25. Kui, S.C.F.; Law, Y.-C.; Tong, G.S.M.; Lu, W.; Yuen, M.-Y.; Che, C.-M. Spectacular Luminescent Behaviour of Tandem Terpyridyl Platinum(II) Acetylide Complexes Attributed to Solvent Effect on Ordering of Excited States, “Ion-Pair” Formation and Molecular Conformations. *Chem. Sci.* **2011**, *2*, 221–228. [CrossRef]
26. Yam, V.W.-W.; Chan, K.H.-Y.; Wong, K.M.-C.; Zhu, N. Luminescent Platinum(II) Terpyridyl Complexes: Effect of Counter Ions on Solvent-Induced Aggregation and Color Changes. *Chem. A Eur. J.* **2005**, *11*, 4535–4543. [CrossRef]
27. Bailey, J.A.; Hill, M.G.; Marsh, R.E.; Miskowski, V.M.; Schaefer, W.P.; Gray, H.B. Electronic Spectroscopy of Chloro(Terpyridine)-Platinum(II). *Inorg. Chem.* **1995**, *34*, 4591–4599. [CrossRef]
28. Kato, M.; Kishi, S.; Wakamatsu, Y.; Sugi, Y.; Osamura, Y.; Koshiyama, T.; Hasegawa, M. Outstanding Vapochromism and PH-Dependent Coloration of Dicyano(4,4'-Dicarboxy-2,2'-Bipyridine)Platinum(II) with a Three-Dimensional Network Structure. *Chem. Lett.* **2005**, *34*, 1368–1369. [CrossRef]
29. National Library of Medicine. Available online: <https://pubchem.ncbi.nlm.nih.gov> (accessed on 29 May 2023).
30. Karimi Abdolmaleki, M. *Synthesis, Characterization, Thermodynamic, and Kinetic Studies of Vapochromic Pt(II) Complexes*; University of Cincinnati: Cincinnati, OH, USA, 2018.
31. Taylor, S.D.; Norton, A.E.; Hart, R.T.; Abdolmaleki, M.K.; Krause, J.A.; Connick, W.B. Between Red and Yellow: Evidence of Intermediates in a Vapochromic Pt(II) Salt. *Chem. Commun.* **2013**, *49*, 9161–9163. [CrossRef]

**Disclaimer/Publisher’s Note:** The statements, opinions and data contained in all publications are solely those of the individual author(s) and contributor(s) and not of MDPI and/or the editor(s). MDPI and/or the editor(s) disclaim responsibility for any injury to people or property resulting from any ideas, methods, instructions or products referred to in the content.